Spatiotemporal Independent Component Analysis for the Detection of Functional Responses in Cat Retinal Images

Eduardo S. Barriga*, *Member, IEEE*, Marios Pattichis, *Senior Member, IEEE*, Dan Ts'o, Michael Abramoff, *Member, IEEE*, Randy Kardon, Young Kwon, and Peter Soliz, *Member, IEEE*

***Abstract*—In the early stages of some retinal diseases, such as glaucoma, loss of retinal activity may be difficult to detect with current clinical instruments. Because current instruments require unattainable levels of patient cooperation, high sensitivity and specificity are difficult to attain. We have devised a new retinal imaging system that detects intrinsic optical signals which reflect functional changes in the retina and that do not require patient cooperation. Measured changes in reflectance in response to the visual stimulus are on the order of 0.1%–1% of the total reflected intensity level, which makes the functional signal difficult to detect by standard methods. The desired functional signal is masked by other physiological signals and by imaging system noise. In this paper, we quantify the limits of independent component analysis (ICA) for detecting the low intensity functional signal and apply ICA to 60 video sequences from experiments using an anesthetized cat whose retina is presented with different patterned stimuli. The results of the analysis show that using ICA, in principle, signal levels of 0.1% can be detected. The study found that in 86% of the animal experiments the patterned stimuli effects on the retina can be detected and extracted.**

***Index Terms*—Functional imaging, independent component analysis (ICA), retina, visual stimulation.**

I. Introduction

In the field of ophthalmology, visual field testing (perimetry) is the gold standard for detection and monitoring progression of diseases such as glaucoma. Perimetry is a functional test of the patient's vision intended to detect defects on the visual field map. Unfortunately, perimetry remains a subjective test that requires the patient to make important judgments during the test that can be clouded by anxiety, fatigue, or lack of concentration. As a result, the sensitivity of this test is poor. Investigators have found that over fifty percent loss of ganglion cells is necessary to detect loss of function with perimetry [1]. Low sensitivity and poor repeatability are frequently observed in areas where anatomical damage has occurred.

As early as 1949, Hill and Keynes linked the activity of the nerve cells with changes in their optical properties [2]. In 1986, Grinvald *et al.* showed that changes in the optical properties of the tissue could be used to study the functional architecture of the cortex [3]. Villringer and Chance used near-infrared light to assess brain activity in humans noninvasively through the skull [4]. We have reported on an optical imaging device of retina function (OID-RF) that has been developed to improve the objectiveness and sensitivity of visual testing [5]–[8]. Kardon *et al.* reported the first device to directly image the human retina by recording changes in 700-nm light caused by retinal activation in response to a 535-nm stimulus [5].

As with the visual cortex, in the retina, several factors may affect spectral reflectance. For example, DeLint *et al.* [9] measured spectral changes of the fovea due to dark adaptation. They concluded that characteristics of the slow reflectance changes suggest changes in the index of refraction between the inter-photoreceptor matrix and photoreceptors as the source. Functional changes in the optic disc and radial papillary capillaries due to stimulus of the retina have been attributed as changes in blood flow [10]. Riva *et al.* [10], [11] have investigated flicker-evoked responses of human optic nerve and subfoveal choroidal blood flow. Although optical techniques are mentioned, their approach is primarily based on laser blood flow measurements. Because the retina is highly vascularized and has a particularly high rate of oxidative metabolism, altered hemodynamics can be observed as changes in reflection and absorption cause by a stimulus. Previous studies, such as Riva's [10], [11], have demonstrated a visual stimulus-induced change in blood flow and oxygenation [11]–[13]. The choroidal circulation in the outer retina is known to have a very high flow rate and a small arteriovenous oxygen saturation difference. In contrast, the retinal circulation nourishing the inner retina, including the ganglion cells has a much slower flow rate and a high arteriovenous saturation difference [14]. This dichotomy suggests that any optical signal due to oximetry will be dominated by the retinal circulation component, and hence more closely reflect the function of the inner retina activity which is of most interest in clinical applications.

Bizheva *et al.* [15] used a high resolution functional optical coherence tomography (fOCT) imager to measure *in vitro* local

Manuscript received December 14, 2006; revised February 21, 2007. *Asterisk indicates corresponding author*.

*E. S. Barriga is with the Electrical and Computer Engineering Department, University of New Mexico, Albuquerque, NM 87106 USA and also with ORION International Technologies, Inc., Albuquerque, NM 87106 USA (e-mail: sbarriga@orionint.com).

M. Pattichis is with the Electrical and Computer Engineering Department, University of New Mexico, Albuquerque, NM 87106 USA.

D. Ts'o is with the Department of Neuroscience and Physiology, State University of New York (SUNY), Upstate Medical University, Syracuse, NY 13210 USA.

M. Abramoff, R. Kardon, and Y. Kwon are with the University of Iowa, Department of Ophthalmology and Visual Sciences, Iowa City, IA 52242 USA.

P. Soliz is with the VisionQuest Biomedical, Albuquerque, NM 87109 USA.

Digital Object Identifier 10.1109/TMI.2007.897366

changes in tissue reflectivity due to physiological changes in dark-adapted retinas as a result of light stimulation. fOCT scans were acquired from these *in vitro* retinas synchronously with electrical recordings before, during, and after light stimulation. Their research clearly shows the stimulus-related changes in the retinal reflectivity profile of the inner and outer segments of the photoreceptor layer and the plexiform layers. This group conducted experiments to show, through pharmacological inhibition of photoreceptor function, that the origin of the observed optical changes is the altered physiological state of the retina evoked by the light stimulus. These studies have shown conclusively that reflectivity in the inner retina of a vertebrate does result from light stimulation.

Our functional imaging device measures the effects of changes in blood conditions (hemoglobin saturation and volume). Using a functional magnetic resonance imaging (fMRI) technique, blood oxygenation level-dependent (BOLD) [16], Duong *et al.* [17] have measure deoxyhemoglobin changes that are brought about by visual stimuli. Changes in regional deoxyhemoglobin content can be visualized in BOLD images. When the retina is stimulated, retinal blood flow increases disproportionately to overcompensate for the stimulus-induced lowering of the hemoglobin saturation resulting from the neural activity. Duong showed convincingly that hemoglobin saturation conditions do indeed result in a functional signal in the retina. Unfortunately, fMRI is not a convenient clinical device for ophthalmology.

These findings motivate the development of a functional imager of the retina that can, using an instrument suitable for the clinical environment, directly measure spatially resolved retina function. The OID-RF measures the increase or decrease in retinal reflectance due to changes in retinal metabolism thought to be a result of blood oxygen uptake and capillary response due to neural activity resulting from visual stimulation of the photoreceptors in the human retina. The functional measurements are stored as optical recordings (videos). The reflectance measurements recorded in these videos are a mixture of the signal that reflects the neuronal activity (functional signal) and signals related to background unknown sources and noise. Given that measured functional changes in intensity due to visual stimulus are on the order of 0.1%–1% of the background signals, it is difficult to extract the functional response using standard methods, such as first frame subtraction and averaging. Our goal is to extract the functional signal that is masked by other signals present during the process of retinal stimulation. Various approaches have been used to improve the signal-to-noise ratio (SNR) characteristics of the functional signal, such as integrating several sets of measurements to improve the SNR. For humans, it is difficult to collect a large number of data sets requiring an hour or more of imaging. So, it is important to know what the limits of the SNR are that will still allow one to detect the functional signal. To find those limits, a numerical experiment using independent component analysis (ICA) [18] has been devised that integrates experimental data from a cat's retina.

In recent years, ICA has been applied to many biological related problems such as electroencephalography (EEG) data analysis [19], [20], and electrocardiogram (ECG) data analysis [21]. Schiessl *et al.* applied ICA techniques to isolate changes on the brain cortex of a macaque monkey due to visual stimulation [22], [23]. ICA has been applied extensively to detect functional brain activation in fMRI experiments [24]. Park *et al.* [25] have applied ICA to model the role of the visual cortex to locate salient areas in an image. They found that ICA was useful in reducing the redundancy of data or signals from the retina to the visual cortex. They defined the signals based on traditional techniques which use color opponent coding and edge detection to model the output from the retina. The authors of this paper have previously reported on the application of ICA techniques to isolate the changes produced in the retina due to visual stimulation [7], [26]–[28].

The functional signal in response to visual stimulus is localized and, therefore, has a super Gaussian spatial distribution, while the noise and other underlying signals are more evenly distributed throughout the image and therefore have a sub-Gaussian distribution. The validity of the basic ICA assumptions in fMRI has been discussed in [24], [29], and [30] and was found to be applicable to our problem.

In this paper, we demonstrate the application of ICA to a set of *in vivo* data collected in our animal study using the OID-RF instrument to extract the functional signal due to retinal stimulation. In our animal study, we expect the major contributors to the signals will be due to cardiac function, the respiratory cycle, and the evoked response. We note that these components correspond to independent physiological processes that should yield independent signals that are appropriate for ICA. Before attempting to extract the functional signal in the cat, we sought to learn the performance for some of the most popular ICA algorithms, Infomax, Fast-ICA, joint approximate diagonalization of eigenmatrices (JADE), second-order blind identification (SOBI), and extended spatial decorrelation (ESD). To achieve this goal, a set of 2-D spatiotemporal synthetic simulations were generated and processed by these algorithms. After the quantitative analysis of the performance of the ICA algorithms, we choose the three methods that gave the best performance and apply them on data collected in *in vivo* cat experiments [8].

This paper is organized as follows. Section II contains a description of the optical imaging device and how the data set was collected. Section III shows the methods used in the analysis of the synthetically generated data and the live cat data. Section IV describes the performance measurements and synthetic simulation methods used to validate the use of ICA in the data. Section V shows the results obtained by applying the ICA techniques in anesthetized cat data. Discussion of the results and conclusions are given in the last two sections.

II. Materials and Data Collection

The OID-RF is a noninvasive imaging device that measures changes in retinal reflectance that result from changes in the blood oxygen saturation and blood volume when patterned stimuli is applied to the subject's retina [5]. The hypothesis is that a visual stimulus causes the retina to alter its level of blood volume and the ratio of oxygenated hemoglobin (HbO) to deoxygenated hemoglobin (Hb). This has the effect of altering the spectral reflectance characteristics of the retina and in turn

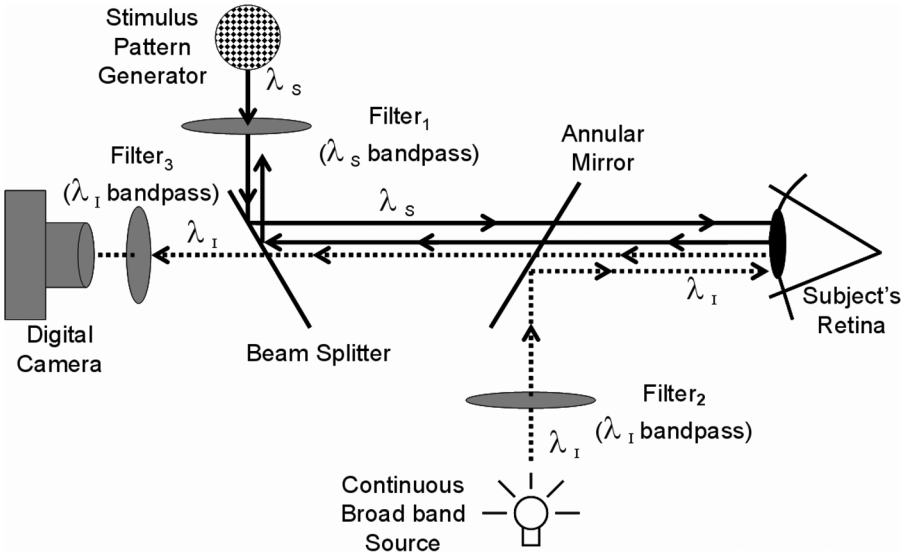

Fig. 1. Optical layout of the OID-RF. Interrogation light at $\lambda_{\mathrm{I}} = 780$–$850\,\mathrm{nm}$ illuminates the retina and is reflected back to the imaging device. patial changes in reflected intensity are affected by the hemodynamics in the retina. Stimulus is presented to the retina at $\lambda_{\mathrm{S}} = 550\,\mathrm{nm}$. Reflected stimulus light is filter out before reaching the imaging camera at filter_3.

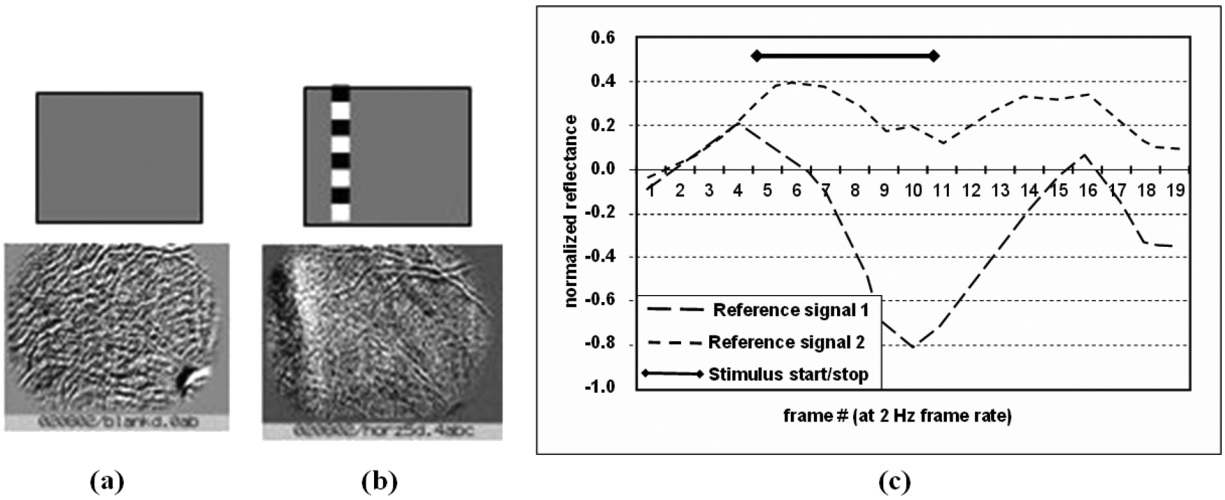

Fig. 2. (a) Prestimulated retina in the interrogation spectral band. (b) Stimulus pattern and response of a live experiment using a cat. (c) Signals for a region within the dark stimulated area (between pixels 21–40 in the x axis) and within the bright stimulated area (between pixels 41–60 in the x axis).

results in a change in the reflected intensity of the image in the stimulated area.

Fig. 1 illustrates the operation the OID-RF. A continuous interrogation light with wavelength in the red-near infrared wavelengths (780–850 nm) is projected onto the subject's retina. Simultaneously, a stimulus pattern at a green wavelength (550 nm) is projected onto the subject's retina. The reflected energy from the retina is then filtered by the beam splitter, which only allows only the interrogation light to be transmitted to the digital recording camera. Kardon *et al.* have previously presented a detailed description of the system [5].

The experimental data were collected from a cat. To avoid artifacts due to eye movements, the cat is anesthetized and immobilized prior to the experiments. A single experiment (epoch) consists of 20 frames of 144 by 192 pixels each, at a frame rate of 2 Hz for a total recording time of 10 s. The stimulus paradigm consists of a checkered pattern with alternating polarity (counter-flickering at 1–20 Hz). Each experiment starts with a baseline (prestimulus) measurement where for the first 2 s the stimulus is turned off. This is followed by a 3 s period of stimulation and 5 s of recovery (poststimulus). The bar-shaped, counter-flickering, checkered stimulus can be applied to a vertical or horizontal region of the retina. Fig. 2(a) is an image of the prestimulated (baseline) retina as measured in the interrogation band (near infrared). Fig. 2(b) shows a vertical counter-flickering stimulus bar with the corresponding measured reflectance of the infrared signal during the maximum functional response signal (about the tenth frame). Fig. 2(c) presents the time plot of the functional response for the stimulated region. The region, which is in the dark response area of Fig. 2(b), is approximately at the second white stimulus box from the top. To the right of the same box another region is sampled that shows a negative response (white region) just outside the stimulated region.

The measured signals in Fig. 2(a) and (c) form the basis of the numerical experiment and simulation. The baseline signal in Fig. 2(a) allows one to estimate the spatial background signal from the prestimulated retina. This signal contains physiological and device noise. The response signal in Fig. 2(c) gives a model of the retinal functional response to the stimulus. A positive or negative gain is applied to this functional response-based model to simulate an experiment with a human subject where the signal has been found to be substantially less than that of the cat. The numerical experiments to be presented in the Section IV are used to establish the detection limits using various signal processing techniques and will aid in defining the experimental protocol for the future human experiments.

III. Methods

Let $X = [x_1(t)x_2(t)\dots x_n(t)]$ be a set of observed random variables and assume that they come from the linear mixture of the components $S = [s_1(t)s_2(t)\dots s_n(t)]$ by a linear mixing matrix A, as in

$$X = AS. \tag{1}$$

Then ICA consists of estimating both A and S using only the observations X and the assumption that the source signals are statistically independent [18]. The statistical independence of the sources means that their joint probability can be factorized as

$$p(S) = \prod_{i=1}^{N} p(s_i) \tag{2}$$

where $p(s_i)$ is the individual probability density function (pdf) of each of the sources and N is the number of sources.

Research in the ICA community has led to the development of a large amount of algorithms, each based on different approaches for maximizing statistical independence of the sources. It is our intention to select a few of the most widely used ICA algorithms and quantify their performances through a series of controlled experiments.

For this study, we selected five different ICA algorithms: Infomax [31], JADE [32], fast-ICA [33], SOBI [34], and ESD [22]. A brief description of how these algorithms work follows.

A. Infomax

The Infomax ICA algorithm was first proposed by Bell and Sejnowski [31] and is a generalization of the Infomax principle applied to ICA. The objective of the Infomax ICA algorithm is to reduce the redundancy between the sources. It is well known from information theory that when a set of signals are statistically independent, their mutual information is zero. As detailed in [35], the mutual information of the sources $I(S)$ is related to the joint entropy $H(g(S))$ of the sources passed through a set of sigmoidal nonlinear functions g_i, as in

$$I(S) = -H\left(g(S)\right) + E\left\{\sum_i \log \frac{|g_i'(s_i)|}{p_i(s_i)}\right\} \tag{3}$$

where $p_i(s_i)$ are the pdf of the sources. $E\{\ \}$ denotes expected value. Some of the most common sigmoidal functions used are the hyperbolic tangent and the cubic power.

If the absolute values of the slopes of the sigmoid functions $|g_i'(s_i)|$ are the same as the independent components pdfs, $p_i(s_i)$ then Infomax (maximization of the joint entropy of the $g(S)$ vector) is the same as ICA (minimization of the mutual information).

Bell and Sejnowski derived a stochastic rule that maximizes the entropy of $g(S)$ using

$$\Delta W \propto (W^{-1})^T + f(s)x^T \tag{4}$$

where W is the estimated inverse of the mixing matrix, $\propto$ means proportionality, and the vector function f has elements

$$f_i(s_i) = \frac{\partial}{\partial s_i} \ln g_i'(s_i). \tag{5}$$

When $g_i'(s_i) = p_i(s_i)$, the ICA algorithm is exact. Of course this leaves the problem that we need to know the pdf of the sources, which in most of the cases is unknown, but a rough approximation of the pdf is sufficient. For a more thorough discussion of how this affects the Infomax algorithm, refer to [20] and [31].

B. JADE

JADE was proposed by Cardoso and Souloumiac in [32] and is based on the joint orthogonalization of the cumulant tensors. The cumulant tensor is defined as a 4-D array whose entries are given by the fourth-order crosscumulants of the data as in

$$Q_x = \{\mathrm{cum}(x_i, x_j, x_k, x_l) | 1 \le i, j, k, l \le n\}. \tag{6}$$

The cumulant matrix $F_{ij}(M)$ associated with any $n \times n$ matrix M (later assumed to be an eigenmatrix) is defined as

$$F_{ij}(M) = \sum_{kl} m_{kl} \mathrm{cum}(x_i, x_j, x_k, x_l) \tag{7}$$

where m_{kl} are the elements of the matrix M. We work with the case that the data follow the ICA model with whitened data

$$x = VAs = W^T s \tag{8}$$

where the whitened matrix is denoted by W^T. Eigenvalue decomposition (EVD) can be viewed as a diagonalization, when the JADE algorithm takes a set of matrices M_i, $i = 1, \dots, m$, and estimates the matrices $C = WF(M_i)W$ as diagonal as possible. The contrast function to measure the diagonality of the matrix C is

$$\phi_{\mathrm{JADE}}(W) = \sum_i \left\|\mathrm{diag}\left(WF(M_i)W^T\right)\right\|^2. \tag{9}$$

After some manipulations [32], the contrast function can be expressed as

$$\phi_{\mathrm{JADE}}(W) = \sum_{i,j,k,l=1,\dots,n} |\mathrm{cum}(y_i, y_j, y_k, y_l)|^2 \tag{10}$$

where $y_i = Wx_i$. Maximization of ϕ_{JADE} is one method of joint diagonalization of $F(M_i)$.

C. Fast-ICA

The Fast-ICA algorithm was developed by Hyvarinen and Oja in [33] and is based on the minimization of gaussianity based on the *negentropy* concept. To define negentropy, we use the concept of differential entropy, defined as

$$S(p_x) = -\int p_x(u)\log p_x(u)du \tag{11}$$

where S is the differential entropy of the random vector X with probability density function p_x. Then, the negentropy is defined as

$$J(p_x) = S(\phi_x) - S(p_x) \tag{12}$$

where ϕ_x is the Gaussian density with the same mean and variance as p_x. The Fast-ICA algorithm then uses a fixed point algorithm to maximize negentropy.

The algorithm then computes the demixing matrix W in an iterative fashion, computing one row at a time using

$$w_i(j+1) = E\left(y\left(w_i^T(j)y\right)^3\right) - 3w_i(j) \tag{13}$$

where $w_i(j+1)$ is the ith row for the $(j+1)$-th iteration and y is the whitened version of the data.

D. SOBI

Our data set contains a temporal structure given by the stimulus and sinusoids. When the independent components are time signals, they may contain much more structure than simple random variables. Some algorithms, like SOBI and ESD try to take advantage of the temporal structure of the data.

A form of the time structure is given by the time-lagged covariance matrix

$$C_\tau^x = E\left\{x(t)x(t-\tau)^T\right\}. \tag{14}$$

When $\tau = 0$, we have the zero-lagged covariance matrix, which only contains second-order information and it is not sufficient for estimating the independent components. Since the sources are assumed to be statistically independent, we know that the lagged covariances are also zero. Thus, we need to estimate a matrix B such that the covariance of $y(t) = Bx(t)$ satisfy

$$E\left\{y_i(t)y_j(t-\tau)^T\right\} = 0, \quad \forall i,j,\tau, i \neq j. \tag{15}$$

Based on this principle, the algorithm for multiple unknown source extraction (AMUSE) [36] was developed. This algorithm is simple and fast to compute but it only works if all the eigenvalues of the time-lagged correlation matrix are different. An extension of the AMUSE algorithm considers different time lags τ instead of just one. The idea is to simultaneously diagonalize all the lagged covariance matrices. A way of measuring the diagonality of a matrix M is to use the operator

$$\mathrm{off}(M) = \sum_{i\neq j} m_{ij}^2 \tag{16}$$

which gives the sum of the squares of the off-diagonal elements of M. What we want is to minimize the sum of the off-diagonal elements of several lagged covariances. For this we use the whitening matrix W and the symmetric version $\overline{C}_\tau^y$ of the lagged covariance matrix. Denoting by S the set of lags τ, we can write the objective function

$$J(W) = \sum_{\tau\in S} \mathrm{off}\left(W\overline{C}_\tau^y W^T\right). \tag{17}$$

Minimizing J under the constraint that W is orthogonal gives us the estimation method. The SOBI algorithm [34] is based on this principle.

E. ESD

The ESD algorithm was proposed by Schiessl *et al.* [22] and is an extension of the AMUSE algorithm (described in Section III-D) for 2-D spatial structures.

ESD minimized the following expression:

$$E_s(W) = \sum_{\Delta r}\sum_{i\neq j}\left(\left(WC(\Delta r)W^T\right)_{i,j}\right)^2 \tag{18}$$

where

$$C_{ij}(\Delta r) = \langle y_i(r)y_j(r+\Delta r)\rangle_r. \tag{19}$$

ESD was applied by Schiessl to optical imaging recordings from the brain cortex of the macaque monkey. Their work included synthetic simulations in two dimensions, but not synthetic video simulations as the one presented in this work.

IV. Performance Measure on Synthetic Data Simulations

In our initial experiments, as well as those of other researchers [4], the amplitude of the reflected signal due to the functional response has been measured to be on the order of 0.1%–1% of the total reflected infrared interrogation light. According to these previous measurements, we have designed a series of experiments to quantify the performance of ICA algorithms in recovering the functional signal. The first experiment consists on synthetic videos generated to assess the capabilities of spatial and temporal estimation of the ICA algorithms. In the second experiment, a hybrid simulation using live data recordings and a synthetically generated stimulus is used to simulate the algorithms' performance under realistic conditions.

Following the approach by Chen and Yao [29], who used cross correlation to select the appropriate independent component, we compare the performance of the ICA algorithms using normalized cross correlation (NCC) as the measure. The criteria for using cross correlation over other performance measures is that since we have both temporal and spatial structure in our data which is well defined in the controlled experiments, correlating the estimated signals with the known original signals gives us an accurate quantification of the performance of the ICA algorithms. It is worth noting that other performance measures [37] were tried, but none of them would asses the accuracy of the spatiotemporal reconstruction of the data. Those performance

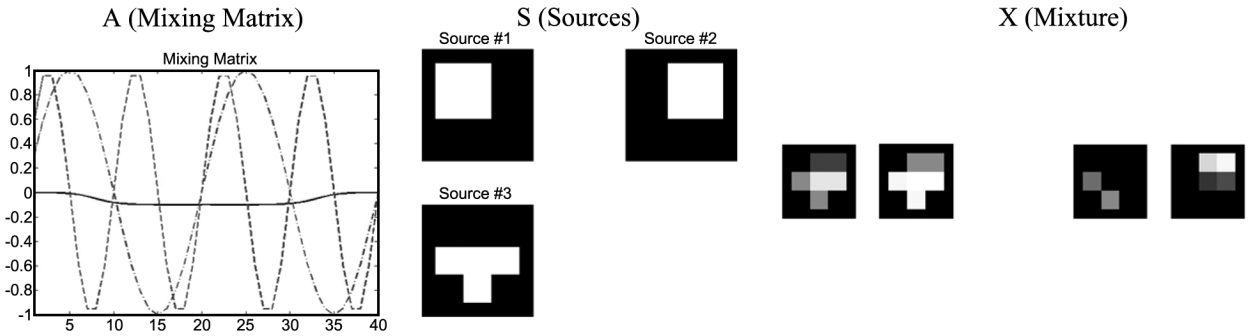

Fig. 3. Signals that form the synthetic video simulation.

measures that are based on the accuracy of the reconstruction of the mixing matrix are not suitable for spatiotemporal datasets.

The NCC of two signals is defined as

$$R_{x,y} = \frac{n\sum xy - \sum x \sum y}{\sqrt{\left[n\sum x^2 - (\sum x)^2\right]\left[n\sum y^2 - (\sum y)^2\right]}}. \quad (20)$$

Since NCC is invariant to scaling, the ambiguity problem of ICA does not affect the results when recovering the independent components. We calculated the NCC for all the combination of reference and estimated signals and pick the highest NCC values. This process will make the order in which the components are extracted not relevant.

A. Synthetic Video Simulation

In the synthetic simulation a video is generated by mixing three images (sources) with a mixing matrix that contains the temporal structures of two sinusoids and a smoothed step function. These sinusoid synthetic signals could represent signals induced by the cardiac cycle and the respiratory cycle. The smoothed step function is generated to simulate an effect similar to the one due to the response to optical stimulation. The step signal amplitude is varied from 10% to 1% of the peak-to-peak amplitude of the other simulated sinusoidal physiological signals. In Fig. 3 we have the representation of the sources, mixing matrix and measurements (video). The images contain 256 pixels each (16×16), the mixing matrix is 3×40 and the mixture results on a video with 40 frames, each with 256 pixels. Note how the white squares in the Fig. 3 were designed to overlap spatially; thus the mixture had regions where there was only one signal, regions with spatiotemporal mixtures of two signals and a region with spatiotemporal mixtures of all the three signals.

We added Gaussian noise to the mixture with an SNR ranging from 40 to 0 dB. By calculating the variance of the original mixture, we generate the appropriate noise level by varying its variance such that

$$\mathrm{SNR}(dB) = 10\log_{10}\frac{\sigma_S^2}{\sigma_N^2} \quad (21)$$

where σ_S^2 is the variance of the original mixture and σ_N^2 is the variance of the Gaussian noise.

After applying the ICA algorithms to this new mixture (the original video plus the noise), we compared the estimated sources and mixing matrix with the originals using the absolute NCC value at zero lag. The sources comparison tells us how accurate the spatial localization is, whereas the mixing matrix comparison establishes the accuracy of the temporal reconstruction.

Fig. 4(a)–(c) show the spatial correlation to a simulated functional response that is modeled as a step source with three different amplitudes, 10%, 5%, and 1% of the total intensity of the images. JADE is the algorithm with the best performance. Even under the most stressing conditions when the functional signal magnitude was only 1% of the other two signals, its spatial correlation never went below 0.8. The Infomax and ESD were clearly the worse performers when measured by NCC. Fig. 4(d)–(f) present the temporal correlations. JADE shows a high correlation value for: SNR greater than 10 dB and a step amplitude of 10%, SNR greater than 20 dB and a step amplitude of 5% and SNR greater than 30 dB and a step amplitude of 1%. The other four algorithms present less than satisfactory results with NCC values of less than 0.5 under all conditions. The Fast-ICA algorithm was used with both deflationary and symmetric decorrelation approaches, but no improvement in the performance was found. The choice of nonlinearity (cubic, hyperbolic tangent, and Gaussian) did not improve its performance.

B. Live Data With Synthetic Stimulus Simulation

The second synthetic simulation involved the mixture of live cat data with a synthetic stimulation. The simulated videos are generated from a live cat experiment where no stimulus was applied, referred to as the baseline video [8]. This baseline video is altered by adding a synthetically generated functional response that is based on the model of an actual response shown in Fig. 2(c). A single video frame during the peak of the functional response in a live cat experiment is shown in Fig. 5(a) and the resulting frames have similar spatial characteristics. Using the baseline video, the model of the functional response is applied. The result is presented in Fig. 5(b). The amplitude of functional response that is added to the baseline video is defined by its stimulus-to-background ratio (SBR)

$$\mathrm{SBR}(dB) = 10\log_{10}\frac{\sigma_S^2}{\sigma_B^2} \quad (22)$$

where σ_S^2 is the variance of the functional signal and σ_B^2 is the variance of the background.

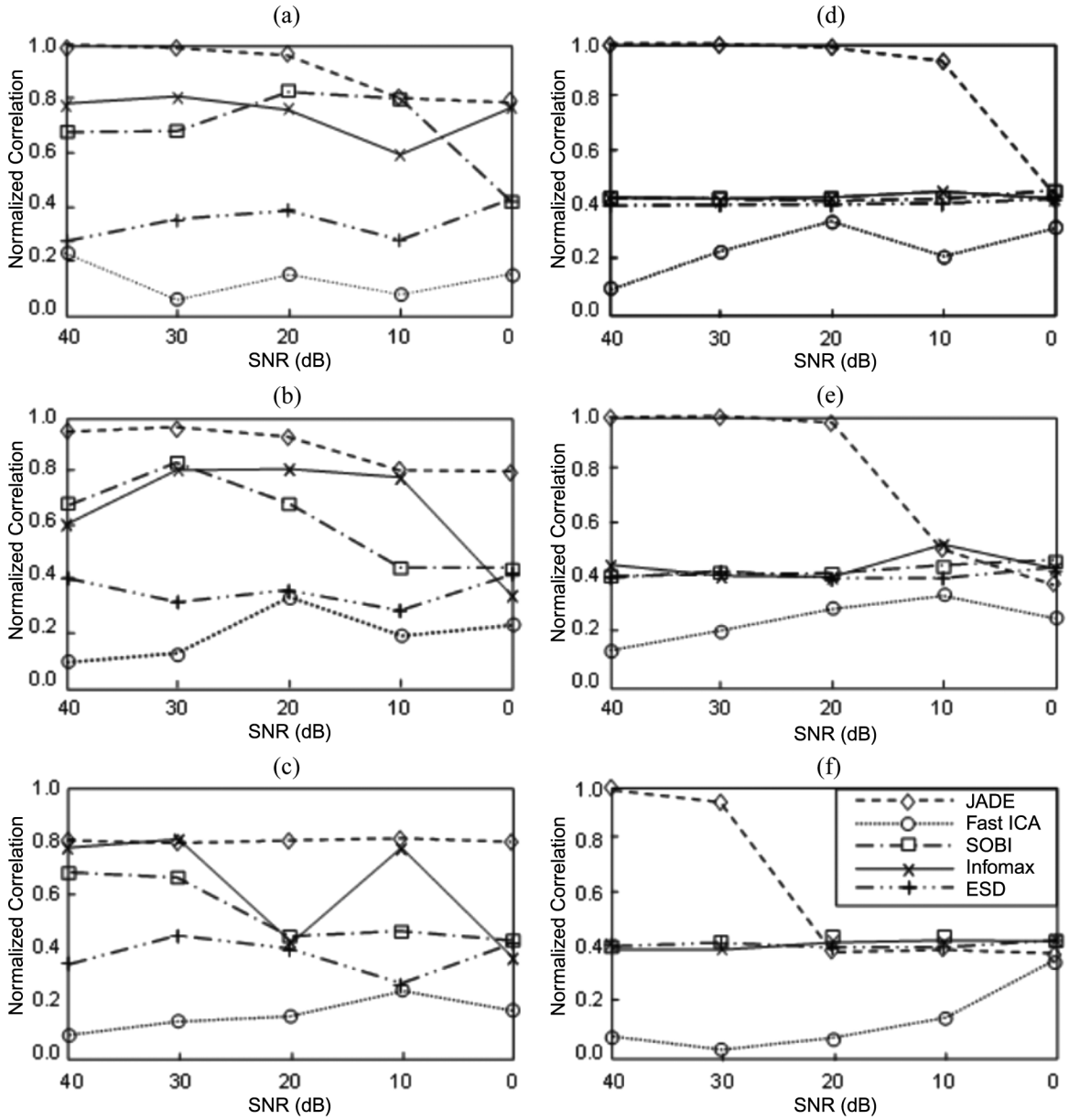

Fig. 4. Spatial and temporal normalized cross correlation results for the step source. Spatial correlations at (a) 10%, (b) 5%, and (c) 1% of the overall intensity level. Temporal correlations at (d) 10%, (e) 5%, and (f) 1% of the overall intensity level.

Five videos were synthesized starting with the SBR ranging from 0 dB to -40 db at -10 dB intervals. Note that the more negative the SBR value, the lower the amplitude of the functional signal. A 0 dB SBR indicates that the variance of the functional signal is equal to the variance of the video, whereas a -30 dB SBR means that the variance of the functional signal is 0.1% of the variance of the video.

The ICA model is now defined as

$$X_{20\times 27648} = \hat{A}_{20\times 3}\hat{S}_{3\times 27648} \tag{23}$$

where the dimensions of the observations X correspond to 20 frames (images) of 144 by 192 pixels each (27648 total pixels). We arbitrarily choose the number of estimated sources to be three, since we are interested in finding two temporal responses and need an extra one to represent any other underlying processes and noise. The analysis was repeated for different number of independent components, but results were similar. Therefore, the estimated mixing matrix $\hat{A}$ will have three column vectors of 20 points each, which will represent the time courses of the independent components. The estimated sources matrix $\hat{S}$ is composed of three row vectors, each of which will generate a 144 $\times$ 192 pixels image. These images are the ones that will give us the spatial distribution of the functional response.

Specifically, the results of the ICA algorithms were compared in the temporal and spatial domains. For the spatial domain, we correlated the sources as estimated by the ICA algorithm with a "reference frame," which is an image artificially generated by using a frame of prestimulated retina and the artificial stimulus on top, as seen in Fig. 5(b). For the temporal comparison, each

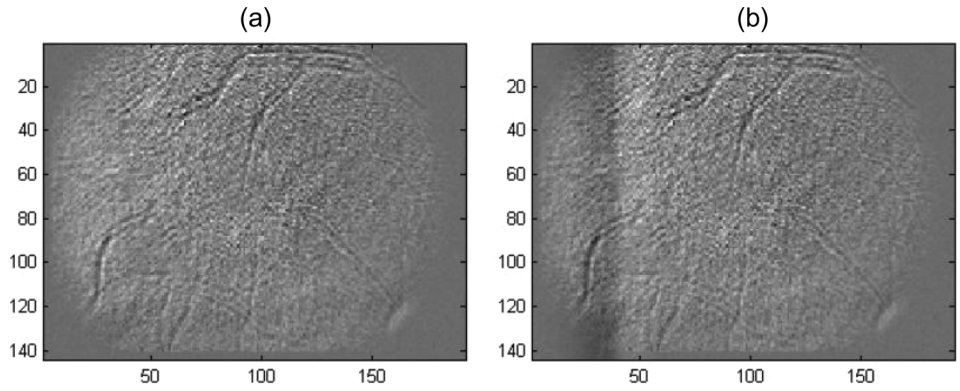

Fig. 5. (a) Live experiment data frame. (b) Synthetically generated image with live data plus synthetically generated stimulation.

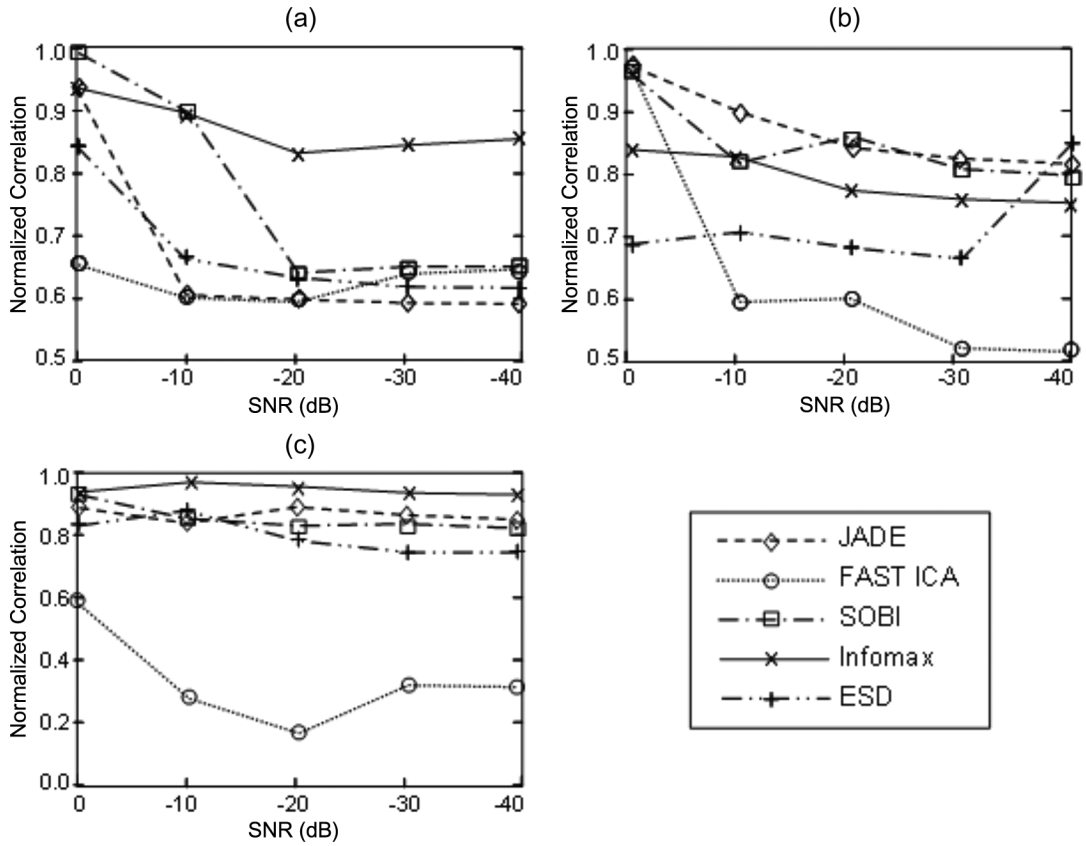

Fig. 6. Temporal and spatial correlation results for live data plus synthetic stimulation experiments. (a) Temporal correlation results using the temporal reference 1 [from Fig. 2(c)]. (b) Temporal correlation results using the temporal reference 2 [from Fig. 2(c)]. (c) Spatial correlation results using the reference frame [from Fig. 5(b)].

row of the estimated mixing matrix $\hat{A}$ was correlated with the modeled functional responses shown previously in Fig. 2(c). A high correlation means that the estimated mixing matrix is following the time trace of the functional response expected due to visual stimulation.

Fig. 6 shows the maximum absolute correlation values at zero lag for (a) temporal reference signal 1 in Fig. 2(c), i.e., the functional response as measured in the bright area of the retina, (b) temporal reference signal 2 in Fig. 2(c), i.e., the functional response as measured in the dark are of the retina, and (c) reference frame Fig. 5(b). From the plots on Fig. 6(a) and (b), one can see that Infomax performs the best for temporal correlation to reference signal 1, whereas JADE and SOBI have the best performance for temporal reference signal 2. ESD and Fast-ICA have performances inferior to the rest, as was the case for the synthetic video simulations. The spatial correlation results shown in Fig. 6(c) show how all the algorithms except Fast-ICA achieve good localization of the stimulus signal, with correlation values between 0.8 and 1 for the different SBR values.

V. *In Vivo* Cat Data Analysis

In the application of ICA algorithms to real data, it is important to address the problem of how to set the number of compo-

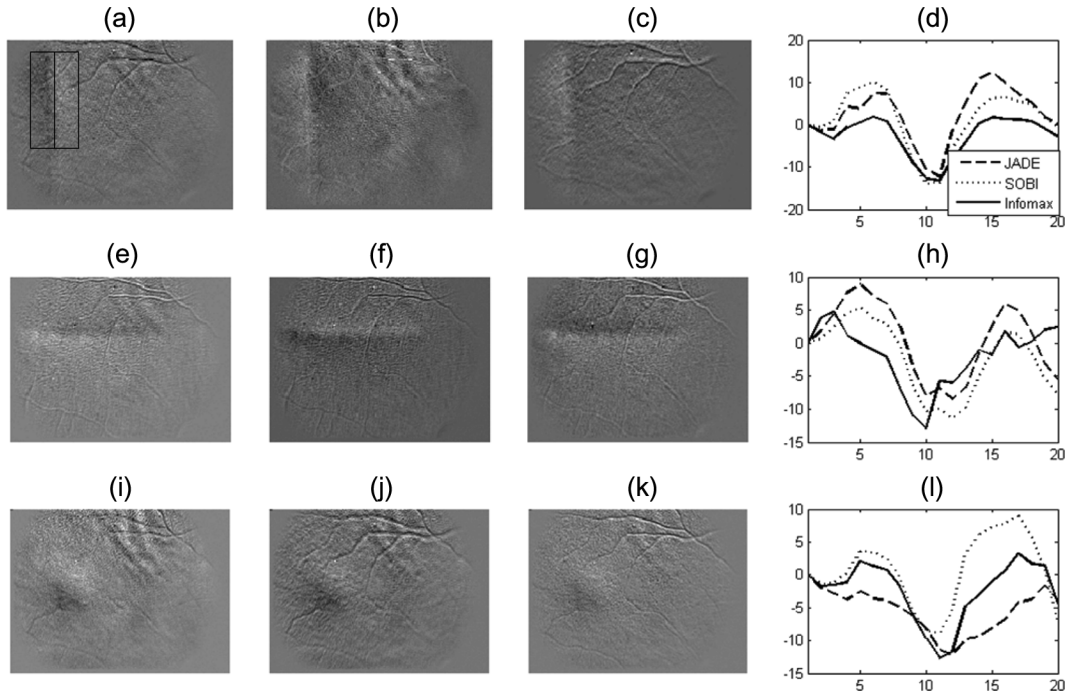

Fig. 7. *In vivo* cat data ICA analysis. (a) Vertical stimulus as estimated by JADE. Overlaid box shows the dark response region (left) and the bright response region (right.) (b) Vertical stimulus estimated by SOBI. (c) Vertical stimulus estimated by Infomax. (d) Time courses of the retinal response to the stimulus estimated by JADE, SOBI, and Infomax. (e)–(h) Horizontal stimulus responses as estimated by JADE, SOBI, and Infomax. (i)–(l) Spot stimulus responses. Note the lower triangular dark response region and the upper triangular bright response region.

nents. For addressing this issue, we run the algorithms for combinations from two to nine components. We then visually inspected all the extracted components for components that were correlated with the stimulus, the unstimulated retinal video images and any other signal pattern that may be due to other physiological effects. Consistently, we found that all algorithms appeared to extract three meaningful components that met these expectations.

Using the results of the synthetic simulations, we narrow the number of ICA algorithms to test on the cat data recordings to three: JADE, Infomax, and SOBI. A single anesthetized cat was used to collect 60 sets of data. Of the 60 data sets, 18 were a vertical stimulus [Fig. 7(a)–(c)], 18 were a horizontal stimulus [Fig. 7(e)–(g)], three were a spot stimulus [Fig. 7(i)–(k)], three were a full field stimulus, and 18 are unstimulated. We successfully extract the stimulus signals in 36 out of the 42 stimulated videos (86%).

Fig. 7 shows a comparison of how the three algorithms extract the stimulus signal spatially and temporally for three different types of stimulation. Fig. 7(a)–(c) show how the ICA algorithms locate the functional response to the vertical stimulus. Fig. 7(d) shows the timelines of these estimated components, as given by the estimated mixing matrices. Note how all three algorithms show a decrease in the reflectance when the stimulus is applied (around frame #5). The decreased reflectance is due to the decrease in blood saturation, which has a larger extinction coefficient that saturated hemoglobin. The decreased reflectance is also a result of increased blood volume in the area being stimulated. The evoked response peaks after 2–2.5 s after the start of the stimulation (frames 10 or 11). After reaching this negative peak, the reflectance starts to increase again eventually returning to its original level. The results for the horizontal and spot stimuli in Fig. 7(e)–(h) and Fig. 7(i)–(l) show the same behavior as when the vertical stimulation is applied to the cat's retina.

Fig. 7(a) marks the region where the stimulus was applied. The rectangular box drawn on top of the cat's retinal image has been divided in two halves; in the leftmost one, a dark response to the stimulus is noted (reference signal 1), and the rightmost box has a bright response (reference signal 2).

The images in Fig. 7 clearly depict the response to counter flickering checkerboard stimulation. Regardless of the shape of the stimuli and their location on the retina, an evoked response was observed (Fig. 7). Interestingly, the stimuli evoked both activation (dark) and inhibition (white). These observations indicate that the retina does not process the incoming complex visual information in a simple manner. The reason for the inhibitory response has not been determined.

VI. Discussion

For the cat experiments, it is clear that, no matter which stimulation condition occurred, visual stimulation evoked a very similar time course in the activated area. The signal changes started immediately after stimulus presentation and reached their peak in about 5 s.

The synthetic stimulus simulations have provided a means to assess the feasibility of extracting a low amplitude functional signal in noisy reflectance images. The results, as presented in Fig. 4, of the spatial correlation of the estimated sources with the reference frame show that the Infomax, JADE and SOBI algorithms achieve the highest correlation values. At the lowest

amplitude of the functional signal [1% in Fig. 4(c)], JADE consistently reproduces the signal at NCC values greater than 0.8. Fast ICA and ESD produce poor results for all magnitudes of the functional signal.

The temporal correlations using cat data and simulated response and physiological signals were given in Fig. 6. This figure shows how well all the algorithms except Fast ICA estimate the functional signals in the dark (reference signal 1) and bright (reference signal 2) response regions where the functional response is located. The functional responses for these two regions are slightly different, with the dark response region peaking negatively very fast and the bright response region increasing its reflectance for about one second to then show a decrease in reflectance similar to the one in the dark region. The correlation results show that Infomax is the algorithm that achieves the best results for the reference signal 1, which was taken from the dark response region Fig. 6(a). For SBR levels higher than -10 dB, JADE and SOBI also achieve high correlation values, but then those values sharply decrease when the SBR is lower than -20 dB. In contrast, when we compare the results of the reconstruction of the bright response region Fig. 6(b), SOBI and JADE outperform Infomax, although not by much. We can hypothesize that SOBI performs better in this case because the reference signal has a more deterministic time structure, and since SOBI takes advantage of the time structure of the components it achieves those high correlation values. It is unclear why JADE performs better in this case, but we have observed that JADE is very consistent on the correlation values obtained, continually having high enough values for detection of the functional signals. In the temporal experiment, we again noted marginal performance by ESD and poor performance by Fast-ICA, which might be due to poor convergence for these specific types of signals or because of the dimensionality of the problem.

When analyzing the live cat data recordings we note several interesting results. First, it is clear how, as a result of the stimulation, two adjacent regions of contrasting reflectance are created. In the case of the vertical stimulation, the dark response region is left to the bright response region. When there is horizontal stimulation, the bright response region is on top of the dark response region. Most interestingly, when there is a spot stimulation (small square), the left/bottom part of the square (lower triangle) forms the dark response region and the right/upper part of the square (upper triangle) forms the bright region, as if the responses of the vertical and horizontal stimulations were additive. Another interesting result is the way the functional response changes the reflectance through time [see Fig. 7(i) and (j)]. At first when the stimulus is applied (frame 5), there is a slight increase in reflectance but then immediately it starts to decrease, to reach its negative peak between frames 10–12 (2–3 s after the start of stimulation). After this negative peak the signal goes back up to higher levels than the original ones to finally come back to the original state after the stimulus is turned off. These results are consistent with other hemodynamical processes observed in the brain using techniques such as fMRI and functional near infrared imaging (fNIR).

VII. Conclusion

We have demonstrated that noninvasive optical imaging of intrinsic signals in the retina reveals a spatial distribution of activity-dependent signals that is highly correlated with the pattern of visual stimulus presented to the retina. Our experimental data indicate that there are several different signals that differ in amplitude, time course, sign, and spatial distribution. The most prominent signal has properties similar to the hemodynamic signals that we and others have previously reported in stimulus activated mammalian sensory cortex. In particular, these signals have a rise time of 1–3 s, an amplitude of 0.01%–0.1%, and are negative in sign (representing a reflectance decrease). Further research will be required to determine the source and anatomic origins of these signals.

The experiments preformed by applying a synthetically generated functional response on top of an image of an unstimulated cat retina have provided us with information of the limits of detection achievable by the ICA algorithms. Our goal was to detect functional responses on the order of 0.1% (-30 dB SBR) of the total reflected signal. Our results show how three ICA algorithms: JADE, Infomax, and SOBI produce estimates of the functional signals that are highly correlated with our references. This study will be more useful when analyzing data from human experiments, since in the human case the functional response is much lower than in the cat; because of more noise sources such as movement (the cat is anesthetized during the experiments, the human is not), lack of focus (the human subject cannot withstand long periods of stimulation), and the complexity of the human retina.

The analysis of the cat data recordings corroborate the findings of the synthetic simulations, and also shows some interesting results such as the generation of a dark/bright contrasting response regions where the retina is stimulated and a time response that follows the same pattern as well known neurophysiological processes studied with fMRI [10], [16], [17]. Our study shows conclusively that even signals as low as 1% or the total reflected near infrared energy can be detected through judicious application of ICA techniques. Our research has set the stage for collecting and analyzing human subject data to measure directly the neurovascular coupling in the human retina. Our observations of the cat data support other studies that suggest an effect of retinal neural activity on hemodyanmics in the retina. Putative mediators underlying this neurovascular response is not within the purview of this paper, but the imaging system and associated ICA methodology will enable the study of these factors.

In conclusion, the OID-RF has been demonstrated to produce a functional response in the cat retina due to visual stimulation. The analysis of the synthetic experiments has given us useful information in determining the threshold of stimulation that can be detected using the ICA algorithms. The analysis of these experiments should also be applicable to any area where we have spatiotemporal responses. It is our intention to apply the results of this study in data from human experiments obtained by a new prototype of the OID-RF device [6].

REFERENCES

[1] H. A. Quigley, G. R. Dunkelberger, and W. R. Green, "Retinal ganglion cell atrophy correlated with automated perimetry in human eyes with glaucoma," *Am. J. Ophthalmol.*, vol. 107, pp. 453–464, 1989.

[2] D. K. Hill and R. D. Keynes, "Opacity changes in stimulated nerve," *J. Physiol.*, vol. 108, pp. 278–281, 1949.

[3] A. Grinvald, E. Lieke, R. D. Frostig, C. D. Gilbert, and T. N. Wiesel, "Functional architecture of cortex revealed by optical imaging of intrinsic signals," *Lett. Nature*, vol. 324, pp. 361–364, 1986.

[4] A. Villringer and B. Chance, "Noninvasive optical spectroscopy and imaging of human brain function," *Trends Neurosci.*, pp. 435–442, 1997.

[5] R. Kardon, Y. H. Kwon, P. W. Truitt, S. C. Nemeth, D. Ts'o, and P. Soliz, "Optical imaging device of retinal function," in *Proc. SPIE Ophthalmic Technologies XII*, 2002, vol. 4611, pp. 230–238.

[6] M. D. Abramoff, Y. H. Kwon, D. Ts'o, P. Soliz, B. Zimmerman, J. Pokorny, and R. Kardon, "Visual stimulus induced changes in human near-infrared fundus reflectance," *Investigative Ophthalmol. Visual Sci. (IOVS)*, vol. 47, pp. 715–721, 2006.

[7] E. S. Barriga, M. S. Pattichis, D. Y. Ts'o, Y. Kwon, R. Kardon, M. D. Abramoff, and P. Soliz, "Detection of low amplitude, in-vivo intrinsic signals from an optical imager of retinal function," *Proc. SPIE Ophthalmic Technologies XVI*, vol. 6138, pp. 66–77, 2006.

[8] D. Y. Ts'o, H. Li, Y. H. Kwon, P. Truitt, and P. Soliz, "Intrinsic signal optical imaging of retinal responses to patterned stimuli," *Investigative Ophthalmol. Visual Sci. (IOVS)*, vol. 43, 2003.

[9] P. J. DeLint, J. M. Berendschot, J. van de Kraats, and D. van Norren, "Slow optical changes in human photoreceptors induced by light," *Investigative Ophthalmol. Visual Sci. (IOVS)*, vol. 41, pp. 282–289, 2000.

[10] C. E. Riva, E. Logean, and B. Falsini, "Visually evoked hemodynamical response and assessment of neurovascular coupling in the optic nerve and retina," *Progress Retinal Eye Res.*, vol. 24, pp. 183–215, 2005.

[11] C. E. Riva, S. D. Cranstoun, J. E. Grunwald, and B. L. Petrig, "Choroidal blood flow in the foveal region of the human disc," *Investigative Ophthalmol. Visual Sci. (IOVS)*, vol. 35, pp. 4273–4281, 1994.

[12] B. Falsini, C. E. Riva, and E. Logean, "Flicker-evoked changes in human optic nerve blood flow: Relationship with retinal neural activity," *Investigative Ophthalmol. Visual Sci. (IOVS)*, vol. 43, pp. 2309–2316, 2002.

[13] R. A. Linsenmeier and L. Padnick-Silver, "Metabolic dependence of photoreceptors on the choroid in the normal and detached retina," *Investigative Ophthalmol. Visual Sci. (IOVS)*, vol. 41, pp. 3117–3123, 2000.

[14] I. M. H. van Buggenum, G. L. Van der Heijde, G. J. Tangelder, and J. W. M. Reichert-Thoen, "Ocular oxygen measurement," *Br. J. Ophthalmol.*, vol. 80, pp. 567–573, 1996.

[15] K. Bizheva, R. Pflug, B. Hermann, B. Povazay, H. Sattmann, P. Qiu, E. Anger, H. Reitsamer, S. Popov, J. R. Taylor, A. Unterhuber, P. Ahnelt, and W. Drexler, "Optophysiology: Depth-resolved probing of retinal physiology with functional ultrahigh-resolution optical coherence tomography," in *Proc. Nat. Acad. Sci. USA*, 2006, vol. 103, pp. 5066–5071.

[16] S. Ogawa, D. W. Tank, and R. Menon, "Intrinsic signal changes accompanying sensory stimulation: Functional brain mapping with magnetic resonance imaging," *Proc. Nat. Acad. Sci. USA*, vol. 89, pp. 5951–5955, 1992.

[17] T. Q. Duong, S.-C. Ngan, K. Ugurbil, and S.-G. Kim, "Functional magnetic resonance imaging of the retina," *Investigative Ophthalmol. Visual Sci. (IOVS)*, vol. 43, pp. 1176–1181, 2002.

[18] A. Hyvarinen, J. Karhunen, and E. Oja, *Independent Component Analysis*. New York: Wiley, 2001.

[19] S. Makeig, A. J. Bell, T.-P. Jung, and T. J. Sejnowski, "Independent component analysis of electroencephalographic data," in *Advances in Neural Information Processing Systems*. Cambridge, MA: MIT Press, 1996, pp. 145–151.

[20] T.-P. Jung, C. Humpries, T.-W. Lee, M. J. McKeown, V. Iragui, S. Makeig, and T. J. Sejnowski, "Removing electroencephalographic artifacts by blind source separation," *Psychophysiology*, vol. 37, pp. 163–178, 2000.

[21] S. Choi, A. Cichocki, and S. Amari, "Fetal electrocardiogram data analysis via flexible independent component analysis," presented at the 4th Asia–Pacific Conf. Med. Bio. Eng. (APCMBE'99), Seoul, Korea, 1999.

[22] I. Schiessl, M. Stetter, J. E. W. Mayhew, N. McLoughlin, J. S. Lund, and K. Obermayer, "Blind signal separation from optical imaging recordings with extended spatial decorrelation," *IEEE Trans. Biomed. Eng.*, vol. 47, no. 5, pp. 573–577, May 2000.

[23] M. Stetter, I. Schiessl, T. Otto, F. Sengpiel, M. Hübener, T. Bonhoeffer, and K. Obermayer, "Principal component analysis and blind separation of sources for optical imaging of intrinsic signals," *NeuroImage*, vol. 11, pp. 482–490, 2000.

[24] V. D. Calhoun and T. Adali, "Unmixing fMRI with independent component analysis," *IEEE Eng. Med. Biol.*, vol. 25, no. 2, pp. 79–90, Mar./Apr. 2006.

[25] S.-J. Park, K.-H. An, and M. Lee, "Aliency map model with adaptive masking based on independent component analysis," *Neurocomputing*, vol. 49, pp. 417–422, 2002.

[26] E. S. Barriga, D. Y. Ts'o, M. S. Pattichis, and P. Soliz, "Independent component analysis for processing of retinal responses to patterned stimuli," in *Proc. 25th Annu. Int. Conf. IEEE Eng. Med. Biol. Soc.*, Sep. 2003, vol. 1, pp. 1006–1009.

[27] E. S. Barriga, P. W. Truitt, M. S. Pattichis, D. Ts'o, R. H. Kwon, R. H. Kardon, and P. Soliz, "Blind source separation in retinal videos," *Proc. SPIE Med. Imaging. 2003 Image Process.*, vol. 5032, pp. 1591–1601, 2003.

[28] E. S. Barriga, P. Soliz, and P. W. Truitt, "Functional signal detection in retinal videos," in *2002 45th Midwest Symp. Circuits Syst. 2002. MWSCAS-2002*, 2002, vol. 1, pp. I-443–I-446.

[29] H. Chen and D. Yao, "Discussion on the choice of separated components in fMRI data analysis by spatial independent component analysis," *Magn. Resonance Imag.*, vol. 22, pp. 827–833, 2004.

[30] M. J. McKeown and T. J. Sejnowski, "Independent component analysis of fMRI data: Examining the assumptions," *Human Brain Mapp.*, vol. 5, pp. 368–372, 1998.

[31] A. J. Bell and T. J. Sejnowski, "An information-maximization approach to blind separation and blind deconvolution," *Neural Computation*, vol. 7, pp. 1003–1034, 1995.

[32] J. Cardoso, "Infomax and maximum likelihood for blind source separation," *IEEE Signal Process. Lett.*, vol. 4, no. 4, pp. 112–114, Apr. 1997.

[33] A. Hyvarinen and E. Oja, "A fast fixed point algorithm for independent component analysis," *Neural Computation*, vol. 9, pp. 1483–1492, 1997.

[34] A. Belouchrani, K. Abed-Meraim, J. Cardoso, and E. Moulines, "A blind source separation technique using second-order statistics," *IEEE Trans. Signal Process.*, vol. 45, no. 2, pp. 434–444, 1997.

[35] T. P. Jung, S. Makeig, M. J. Mckeown, A. J. Bell, T. W. Lee, and T. J. Sejnowski, "Imaging brain dynamics using independent component analysis," *Proc. IEEE*, vol. 89, no. 7, pp. 1107–1112, Jul. 2001.

[36] L. Molgedey and H. G. Schuster, "Separation of a mixture of independent signals using time delayed decorrelations," *Phys. Rev. Lett.*, vol. 72, 1994.

[37] A. Mansour, M. Kawamoto, and N. Ohnishi, "A survey of the performance indexes of ICA algorithms," in *Proc. 21st IASTED Int. Conf. Modeling, Identification Control (MIC '02)*, 2002, pp. 660–666.